Published in final edited form as:
Clin Cancer Res. 2010 December 15; 16(24): 6049–6059. doi:10.1158/1078-0432.CCR-10-2435.

Microenvironmental regulation of glioblastoma radioresponse

Muhammad Jamal, **Barbara H. Rath**, **Eli S. Williams**, **Kevin Camphausen**, and **Philip J. Tofilon**
Drug Discovery Department, Moffitt Cancer Center, Tampa, FL (MJ, BHR, ESW, PJT) Radiation Oncology Branch, National Cancer Institute, Bethesda, MD (KC)

Abstract

Purpose—Brain tumor xenografts initiated from human glioblastoma (GBM) stem like cells (TSCs) simulate the biological characteristics of GBMs *in situ*. Therefore, to determine whether the brain microenvironment affects the intrinsic radiosensitivity of GBM cells, we compared the radioresponse of GBM TSCs grown *in vitro* and as brain tumor xenografts.

Experimental Design—As indicators of DNA double strand breaks (DSBs), γH2AX and 53BP1 foci were defined after irradiation of two GBM TSC lines grown *in vitro* and as orthotopic xenografts in nude mice. Microarray analysis was performed to compare gene expression patterns under each growth condition.

Results—Dispersal of radiation-induced γH2AX and 53BP1 foci was faster in the tumor cells grown as orthotopic xenografts compared to cells irradiated *in vitro*. In addition, cells irradiated *in vivo* were approximately 3-fold less susceptible to foci induction as compared to cells grown *in vitro*. Microarray analysis revealed a significant number of genes whose expression was commonly affected in the two GBM models by orthotopic growth conditions. Consistent with the decrease in sensitivity to foci induction, genes related to ROS metabolism were expressed at higher levels in the brain tumor xenografts.

Conclusion—γH2AX and 53BP1 foci analyses indicate that GBM cells irradiated within orthotopic xenografts have a greater capacity to repair DSBs and are less susceptible to their induction than tumor cells irradiated under *in vitro* growth conditions. Because DSB induction and repair are critical determinants of radiosensitivity, these results imply that the brain microenvironment contributes to GBM radioresistance.

Keywords

microenvironment; glioblastoma stem cells; radiosensitivity; γH2AX; orthotopic xenografts

Introduction

Radiotherapy remains a primary treatment modality for glioblastomas (GBMs); yet, whereas many GBMs initially respond, the vast majority recurs within 2 years of diagnosis (1). Given that increased total dose fails to improve local control (2) and that the pattern of failure includes a predominance of recurrence within the initial treatment volume (3) GBM cells *in situ* are considered to be radioresistant. Defining the processes and molecules responsible for this radioresistance should provide a rational basis for designing target based strategies that enhance GBM radiosensitivity and therapeutic response. Investigations aimed at delineating such mechanisms and identifying targets for radiosensitization have generally

Corresponding Author: Philip J. Tofilon, Ph.D., Drug Discovery Department, Moffitt Cancer Center, 12902 Magnolia Drive, SRB3-DRDIS, Tampa, FL 33612, philip.tofilon@moffitt.org.

focused on *in vitro* cultures of long established glioma cell lines. However, the biology of glioma cell lines as reflected by genetic abnormalities, gene expression and orthotopic growth patterns has little in common with GBM *in situ* (4). Moreover, the radiosensitivity of such glioma cells is not significantly different from cell lines initiated from tumor types that typically respond to radiotherapy (5).

With respect to a more biologically accurate model system, data now suggest that GBMs are driven and maintained by a subpopulation of clonogenic cells referred to as tumor stem-like cells (TSCs). The identification and isolation of GBM TSCs has been primarily based on the stem cell associated protein CD133 (6), although additional markers have been reported (7). CD133+ TSCs have a number of *in vitro* properties in common with normal neural stem cells including continuous self renewal; expression of stem cell related genes and the capacity to at least partial differentiate along neuronal and glial pathways (6,8,9). However, in terms of radiosensitivity, we have recently shown that CD133+ TSCs *in vitro* are actually more radiosensitive than established glioma cell lines (10); the applicability of CD133+ TSCs as a model of GBM radioresistance is thus unclear. A parameter that may influence radioresponse and obviously not considered in this initial investigation of GBM TSCs (10) is the brain microenvironment. In contrast to the traditional GBM cell lines, when implanted into the brains of immuno-compromised mice TSCs grow as invasive neoplasms comprised of heterogeneous subpopulations (6,8,9,11–13). Moreover, brain tumor xenografts initiated from TSCs simulate the genotype and gene expression patterns of the GBM from which they originated (9,12). Given that TSC initiated intracerebral (ic) xenografts replicate the genotype, phenotype and *in vivo* growth pattern of GBMs, we reasoned that they are also likely to reflect the potential influence of the microenvironment on GBM radiosensitivity.

Identifying a role for the microenvironment in GBM radioresponse requires a measure of intrinsic radiosensitivity that allows for the direct comparison between cells grown *in vitro* and as tumor xenografts. In contrast to tumor growth rate and animal survival, an indicator of radiosensitivity defined at the individual cell level and applicable to *in vitro* and *in vivo* models is γH2AX foci expression. It is well established that γH2AX foci correspond to radiation-induced DNA double strand breaks (DSBs) and that their dispersal correlates with DSB repair (14,15). Because DSBs are the critical lesion in radiation-induced cell death, γH2AX foci also provide a measure of radiosensitivity (16–18). To determine whether the microenvironment influences the intrinsic radiosensitivity of GBM cells, we have used γH2AX foci to directly compare the radioresponse of GBM TSCs grown *in vitro* and as ic xenografts. Data presented show that the initial level of radiation-induced γH2AX foci was significantly reduced in tumor cells within ic xenografts and the foci that did form dispersed more rapidly as compared to cells irradiated under the *in vitro* conditions. These results thus imply that GBM cells grown ic are less susceptible to DSB induction and have an increased capacity to repair DSBs, which then suggests that the brain microenvironment contributes to GBM radioresistance.

Materials and Methods

GBM TSC culture

Neurosphere forming cultures NSC11 and GBMJ1 were isolated from two human GBM surgical specimens as described previously (10,19). NSC11 was kindly provided by Dr. Frederick Lang (M. D. Anderson Cancer Center) and GBMJ1 was generated at Moffitt Cancer Center from surgical specimen classified as glioblastoma according to WHO criteria (20) and was obtained following informed consent in accordance with the local institutional review board. Neurospheres were maintained in medium consisting of DMEM/F-12 (Invitrogen, Carlsbad, CA), B27 supplement (1X; Invitrogen) and human recombinant bFGF and EGF (50 ng/ml each, R&D Systems, Minneapolis, MN). To dissociate neurospheres into

single cells, spheres were treated with TryplE Express (Invitrogen) for 5 minutes at 37°C, then subjected to mechanical disaggregation and strained through a 40 μm cell strainer (BD, Franklin Lakes, NJ). All cultures were maintained at 37°C in an atmosphere of 5% CO_2/7% O_2 (21).

CD133+ cells were isolated from NSC11 and GBMJ1 neurosphere cultures by FACS as previously described (10). Both $CD133^+$ cell cultures met the criteria for tumor stem-like cells (6) including self-renewal, differentiation along glial and neuronal pathways, expression of stem cell related genes and formation of brain tumors when implanted in immunodeficient mice(10,21). For use in an *in vitro* experiment, CD133+ neurosphere cultures were disaggregated into single cells and seeded into poly-L-lysine coated plates in neural basal media containing EGF and bFGF, i.e. stem cell growth media. Under these conditions the TSCs grow as an adherent monolayer maintaining their CD133 expression and stem-like characteristics (10) To induce differentiation and cell cycle arrest, CD133+ cell were exposed to medium consisting DMEM/F-12 and 10% fetal bovine serum (FBS) for 10 days. Differentiation was defined as the loss of CD133 expression, the gain of expression of GFAP and/or β-III tubulin and cell cycle arrest.

Generation of intracerebral (ic) xenografts

Athymic nude mice (nu/nu, males, Harlan Laboratories, Indiana, USA) 4–6 weeks of age were used in these studies. To implant tumor cells, mice were anesthetized using isoflurane gas and placed in a small animal stereotactic apparatus (Stoelting, Illinois, USA). 10^5 CD133+ cells were injected in a total volume of 5 μl at 1.0 mm anterior and 2.0 mm lateral to the bregma to a depth of 3.5 mm at a rate of approximately 1μl/min. Mice were kept in the Moffitt Cancer Center animal facility and observed every day until the initial signs of morbidity. All experiments were performed as approved by the Institutional Animal Care and Use Committee (IACUC) and the experiment protocols were approved by the Division of Comparative Medicine, University of South Florida, Tampa, Florida.

Irradiation

For *in vitro* experiments, the CD133+ TSCs in stem cell medium or after differentiation were irradiated as monolayers using XRad 320 X-irradiator (Precision XRay Inc., N. Branford, CT) at 320 kV and a dose rate of 289.8 cGy min^{-1}. For *in vivo* irradiation, mice were anesthetized using a cocktail of Ketamine/Xylazine/Acepromazine and placed in well-ventilated plexiglass jigs with shielding for the entire torso of the mouse along with critical normal structures of the head (e.g. ears, eyes, neck). Irradiation was performed using the same X-ray machine as for the *in vitro* studies at a dose rate of 289.8 cGy min^{-1}. Sham-irradiated mice served as the control group.

Immunofluorescent analyses of γH2AX and 53BP1 foci

For *in vitro* analyses, CD133+ NSC11 and GBMJ1 were seeded onto Lab-Tek CC2-treated tissue culture slides (Thermo Fisher, Rochester, NY) at least 24h before use in an experiment. To visualize foci, cultures were fixed with 4% paraformaldehyde, permeabilized with 0.1% Triton X-100, and blocked with 1% bovine serum albumin (BSA) in PBS containing 5% goat serum. The slides were incubated with primary antibodies (1:1000) to phospho-H2AX (Upstate Biotechnology, Charlottesville, VA)or 53BP1 (BD Transduction Laboratories) overnight at 4°C and followed by secondary antibodies Alexa Fluor 488 goat anti-mouse IgG and Alexa Fluor 594 goat anti-rabbit IgG (1:1000), respectively (Molecular Probes, Eugene, CA, USA), and mounted with Prolong Gold anti-fade reagent containing 4′, 6-diamidino-2-phenylindole (Invitrogen) to visualize nuclei. Cells were analyzed on a Zeiss upright fluorescent microscope. Data presented are the mean ± SD of three independent experiments in which 50 cells were evaluated.

For *in vivo* studies, mice were euthanized by CO_2 inhalation and perfused with 4% paraformaldehyde in PBS (pH 7.4) via cardiac puncture. Brains were then removed and placed in 10% buffered formalin for 48h before embedding in paraffin. The paraffin embedded brains were cut into 10μM thick slices; sections were deparaffinized in xylene and rehydrated in decreasing grades of alcohol. Sections were boiled in citrate buffer and incubated in 1% bovine serum albumin (BSA) in PBScontaining 10% goat serum. The slides were then incubated with primary antibodies to phospho-H2AX (Upstate Biotechnology, 1:500) or 53BP1 (BD Transduction Laboratories, 1:500) for overnight at 4°C followed by secondary antibodies Alexa Fluor 488 goat anti-mouse IgG and Alexa Fluor 594 goat anti-rabbit IgG at 1:500, respectively and mounted with Prolong Gold anti-fade (Invitrogen). Foci analysis was preformed using a Leica confocal microscope (Leica TCS SP5 Confocal, Mannheim, Germany) with evaluation of only non-necrotic tumor tissue. To obtain an accurate foci count, the depth of the nuclei was scanned by focusing manually along the optical axis (z-direction; original magnification, 100x) and images of 10 to 20 slices were recorded per z-stack to map the entire nucleus, essentially as described (18). Data are presented as the mean ± SD of 3–4 mice collected in at least 2 independent experiments in which 50 cells were evaluated.

Statistical analysis

Differences between control and irradiated groups were evaluated according to Student's t-test with statistical significance defined as $p < 0.05$.

Identification of ic xenograft subpopulations

CD133 expression was evaluated in paraffin embedded tissue as described above using a primary antibody against CD133 (Cell Signaling, 1:500) followed by Alexa Fluor 594 goat anti-rabbit IgG (1:500). After washing in PBS, slides were mounted in anti-fade. To better visualize the expression of GFAP and βIII tubulin within brain tumor xenografts, analysis was performed on frozen sections. After cardiac perfusion brains were post-fixed overnight, transferred to 10% sucrose (4°C) followed by 20% sucrose (4°C) and embedded in Tissue-Tek (Sakura, Heppenheim, Germany). Cryostat sections (6μM) were acetone-fixed and blocked in 10% goat serum in 1% BSA for 1h at room temperature and incubated with primary antibodies diluted in 1% BSA [anti-GFAP, 1:200 (Millipore); antiβIII tubulin, 1:500 (Abcam)] followed by incubation with secondary antibodies (goat anti-mouse conjugated to AlexaFluor 488 and Alexa Fluor 594 goat anti-rabbit IgG (1:500), respectively, and mounted in anti-fade. Images were generated using a Leica confocal microscope.

Microarray analysis of gene expression

For microarray analysis, 100 ng of total RNA was collected in replicate from ic tumor xenografts and *in vitro* cultures and converted to cDNA (Ambion). The cDNA samples were amplified and labeled with biotin following the procedure initially described by Van Gelder et al.(22). Hybridization with the biotin-labeled cRNA, staining, and scanning of the microarray chip followed the prescribed procedure outlined in the Affymetrix technical manual as previously described (23). For the oligonucleotide probe arrays, Human Genome U133A 2.0 chips (Affymetrix, Santa Clara, CA) were used having >22000 probesets. The chips were scanned and the output files were visually inspected for hybridization artifacts and then analyzed using Affymetrix Microarray MAS 5.0 software. After MAS 5.0 analysis, effects of *in vivo* growth were determined by dividing the expression levels from a given ic xenograft (*in vivo*) by the corresponding CD133+ or differentiated *in vitro* samples. Fold-changes were uploaded into Gene Cluster software (http://bonsai.hgc.jp/~mdehoon/software/cluster/software.htm), log2 transformed and arranged in a self-organizing map (SOM) (24), which was visualized using the Treeview software (http://bonsai.hgc.jp/~mdehoon/software/cluster/software.htm). Genes that were

differentially expressed *in vivo* as compared to *in vitro* conditions were defined as those with a >2.0 fold-change (increased) and <0.5 fold-change (decreased). The ROS/ARE gene list was generated by combining the gene lists for ROS metabolism (25) and ARE containing genes (26) and consisted of 367 individual genes (Supplemental Table 1). The differentially expressed genes were filtered for those target genes and uploaded into Venn diagrams to show the overlapping increased and decreased genes between each experimental calculation.

Results

NSC11 intracerebral (ic) xenografts

To determine whether the brain microenvironment influences the intrinsic radiosensitivity of GBM cells, we initially focused on ic xenografts initiated from CD133+ NSC11 cells. The intracerebral implantation of CD133+ NSC11 cells into nu/nu mice results in the formation of a highly invasive brain tumor containing cells expressing GFAP, βIII tubulin and CD133 (Fig. 1). Detection of GFAP and βIII tubulin indicates the presence of tumor cells that have differentiated at least partially along astrocytic and neuronal pathways, respectively; CD133 expression suggests the continued presence of TSCs. Whereas 100% of the cells implanted ic were CD133+, at the initial signs of animal morbidity, 11%± 3.3 (mean ± SD, n=3) of the cells within a tumor expressed CD133. Thus, these data indicate that the implanted CD133+ NSC11 cells proliferate and undergo differentiation along both glial and neuronal pathways to form an invasive, phenotypically heterogeneous tumor, i.e., recapitulating GBM in situ.

γH2AX foci after irradiation of NSC11 cells

As an indicator of DSB induction and repair we used γH2AX nuclear foci. Mice bearing NSC11 intracerebral tumors were irradiated (6 Gy) at the initial signs of morbidity and euthanized at times out to 24h. Using 10μ sections,γH2AX foci were quantified in individual nuclei using confocal microscopy and a stacking procedure that allowed for evaluation of whole nuclei in the z-direction. This procedure is necessary to prevent underscoring of foci due to incomplete visualization of the entire nucleus and is essentially as described by Rube et al in their evaluation of γH2AX foci in mouse tissue (18). Only tumor cells in non-necrotic regions of the tumor mass were evaluated; representative composite images of γH2AX foci in control and irradiated NSC11 intracerebral xenograft are shown in figure 2A. The maximum number of γH2AX foci was reached at 0.5h after irradiation followed by a rapid decline at 1h with a further reduction by 6h; at 24h there was no significant difference as compared to control (Fig. 2B).

γH2AX foci levels were also evaluated in NSC11 cells grown in vitro (Fig. 2C). For this analysis two *in vitro* growth conditions were evaluated: CD133+ NSC11 cells maintained in stem cell medium (TSCs) and CD133+ NSC11 cells that had been exposed to 10% FBS for 10 days (differentiated), which results in the loss of CD133 expression and differentiation along astroglial and neuronal pathways (21). Use of both *in vitro* growth conditions thus approximates the phenotypic heterogeneity of the ic xenografts. Moreover, use of both in vitro models addresses the potential contribution of cell cycle phase distribution in radiation-induced γH2AX foci formation, i.e. approximately 2-fold more foci are induced in G2 than in G1 (15). In the differentiated cultures >93% of cells are in G1/G0 versus only ~50% in the CD133+ cultures (data not shown and ref (10)). For differentiated cells in vitro, the number of γH2AX foci induced by radiation (2 Gy) was less than that induced in the CD133+ NSC11 cells at each time point evaluated (Fig 2C), which may be due to the greater percentage of G1/G0 cells. Although γH2AX foci returned to control levels by 24h after irradiation of the differentiated cultures, in the CD133+ TSCs the number remained significantly above control values, similar to our previous results (10). It should be noted that our initial analysis of radiation-induced γH2AX foci in CD133+ GBM TSCs was

performed at 20% oxygen (10); the present results were obtained for cells grown at 7% oxygen (21), which had no significant influence on foci induction or dispersal. Comparison of the time courses shown in figures 2B and C indicates that for cells irradiated as ic xenografts the maximum γH2AX foci dispersal rate occurred between 0.5 and 1h post-irradiation, whereas for both *in vitro* models foci dispersal was relatively steady over the 24h evaluation period. These data suggest that repair of radiation-induced DSBs was considerably more rapid in tumor cells irradiated under orthotopic conditions.

Comparison of figures 2B and C also revealed that 6 Gy delivered to ic xenografts resulted in a similar level of γH2AX foci as induced by 2 Gy *in vitro*. To better illustrate this difference in susceptibility to radiation-induced γH2AX foci the dose response at 0.5h for each growth condition is shown in figure 2D. With respect to *in vitro* growth conditions, the differentiated cultures contained fewer radiation-induced γH2AX foci at each dose tested than the actively cycling CD133+ cultures, again, perhaps due to the differences in cell cycle phase distribution. However, the NSC11 cells grown orthotopically, were substantially less susceptible to γH2AX induction than both *in vitro* culture models.

53BP1 foci after irradiation of NSC11 cells

53BP1 is a critical protein participating in the radiation-induced DNA damage response that also forms nuclear foci after irradiation (27). Although the retention of 53BP1 at foci is facilitated by γH2AX, its initial recruitment to the site of DSBs does not requireγH2AX (28) and thus provides an independent measure of DSB induction (18,28). After irradiation of CD133+ NSC11 initiated xenografts the number of 53BP1 foci reached a maximum at 0.5h followed by a rapid decline at 1h returning to control levels by 6h (Fig. 3A). Irradiation of the NSC11 cells *in vitro* resulted in 53BP1 foci induction and dispersal similar to that detected for γH2AX. For differentiated cells *in vitro*, the number of 53BP1 foci induced by radiation (2 Gy) was less than that induced in the CD133+ NSC11 cells at each time point evaluated (Fig. 3B). By 24h after irradiation 53BP1 foci returned to control levels in differentiated cultures, yet remained significantly above control values in the CD133+ cultures. As compared to ic xenografts, the dispersal of 53BP1 foci after irradiation under both *in vitro* growth conditions was considerably slower, remaining significantly above control levels at 6h (Fig. 3B). Consistent with the γH2AX data, these results suggest that the repair of DSBs is more rapid in NSC11 cells grown orthotopically. In addition, the number of 53BP1 foci induced in both *in vitro* models at 0.5h after 2 Gy was similar to that induced by 6 Gy for cells within the ic xenografts. Thus, tumor cells grown orthotopically were less susceptible to radiation-induced 53BP1 foci formation.

GBMJ1 ic xenografts

To determine whether these results were unique to NSC11 tumors, similar experiments were performed using CD133+ GBMJ1 TSCs. The intracerebral implantation of these cells results in the formation of highly invasive brain tumors with cells expressing GFAP, βIII tubulin as well as CD133 (Fig. 4), similar to NSC11 tumors. Whereas 100% of the GBMJ1 TSCs implanted ic were CD133+, at the initial signs of animal morbidity, the percent CD133+ cells was 9.6% ± 1.5 (mean ± SD, n=3). After irradiation (6 Gy) of ic xenografts, γH2AX foci were readily detectable at 0.5h returning to control levels by 6h (Fig. 5A). These results were then compared to those obtained from GBMJ1 cells maintained under 2 types of *in vitro* growth conditions: CD133+ cells maintained in stem cell medium (TSCs) and CD133+ cells that had been exposed to 10% FBS for 10 days (differentiated) (Fig. 5B). In contrast to NSC11 cells, there was no detectable difference in the radiation-induced γH2AX response of CD133+ and differentiated GBMJ1 cells *in vitro*. Whereas >90% of the cells in the differentiated cultures were in G1/G0 versus ~57% in the CD133+ GBMJ1 cultures (data not shown), additional phenotypic changes may be involved affecting γH2AX induction

under these two *in vitro* conditions. However, similar to the NSC11 model, the dispersal of γH2AX foci was more rapid after irradiation of GBMJ1 ic xenografts as compared to the *in vitro* growth conditions. In addition, the susceptibility of cells grown orthotopically to radiation-induced γH2AX foci was substantially less than for GBMJ1 cells irradiated *in vitro* (2 vs. 6 Gy).

Microenvironmental influence on GBM gene expression

To begin to address the mechanisms responsible for the differences in γH2AX and 53BP1 foci induction as defined above, microarray analysis was used to generate gene expression signatures for NSC11 and GBMJ1 cells grown *in vivo* as ic xenografts and *in vitro* under stem cell and differentiated conditions. To define the changes in gene expression resulting from *in vivo* growth, gene expression signatures of the ic xenografts (*in vivo*) were directly compared to those generated from their corresponding *in vitro* cultures (CD133+ and differentiated). Using these data, a SOM was generated to compare the *in vivo* mediated changes in gene expression induced in the NSC11 and GBMJ1 models (figure 6A). Within the each of the GBM models, there were a significant number of genes in CD133+ and differentiated cultures that were commonly affected by *in vivo* growth. In addition, although there were differences between the GBM models, there were also a significant number of genes similarly affected by *in vivo* growth in both NSC11 and GBMJ1. These results suggest that the effects of brain microenvironment on gene expression are not tumor specific and may be of a more general nature.

The gene expression profiles comparing *in vivo* to *in vitro* growth were then evaluated in terms of genes that can play a role in radioresponse. Of particular interest were genes involved in ROS scavenging and anti-oxidant response, which have long been implicated as determinants of radiosensitivity. Accordingly, gene expression signatures as defined in figure 6A for ic xenografts versus their respective *in vitro* cultures were interrogated using a list of genes associated with ROS metabolism (25) and anti-oxidant response as reflected by an ARE (antioxidant responsive element) containing promoter (Supplemental Table 1) (26). The ROS/ARE genes whose expression was modified at least 2-fold by *in vivo* growth were identified for each *in vitro* growth condition (CD133+ and differentiated) and GBM model (NSC11 and GBMJ1) with similarities depicted in Venn diagrams (figure 6B). Each xenograft contained substantially more up-regulated than down-regulated ROS/ARE genes than their respective in vitro CD133+ cultures; 114 genes were commonly up-regulated (top panel). The xenografts also contained substantially more up-regulated than down-regulated ROS/ARE genes than their respective differentiated *in vitro* cultures; 93 genes were commonly up-regulated (middle panel). To determine whether there were similarities between the two *in vitro* phenotypes in terms of ROS/ARE genes affected by ic growth, the 125 commonly affected genes (up- and down-regulated) identified for ic xenografts versus CD133+ cells (top panel) were compared with the 110 commonly affected genes identified for ic xenografts versus differentiated cells (middle panel). As shown in the bottom panel of figure 6B, 64 ROS/ARE genes expressed in CD133+ and differentiated cells *in vitro* were commonly up-regulated under ic growth conditions in both GBM models, whereas only 3 genes were down-regulated (Supplemental Table 2). These results indicate that a consequence of orthotopic growth of GBM cells is an increased expression of ROS/ARE related genes, which would be consistent with greater anti-oxidant capacity and reduced susceptibility to radiation-induced DSBs.

Discussion

GBMs comprise a diverse set of tumors that are highly variable with respect to histology, genetic abnormalities and gene expression profiles. However, despite their extensive biological heterogeneity, although some GBMs respond better than others, they all

essentially fail radiotherapy (1). This relatively “homogeneous” clinical response in a background of inter-tumor heterogeneity suggests that the microenvironment may play a significant role in determining their radioresponse. The goal of this study was to test the hypothesis that the brain microenvironment contributes to GBM radioresistance. Towards this end it was necessary to directly compare the intrinsic radiosensitivity of cells grown *in vitro* and *in vivo* as orthotopic xenografts.

The gold standard for defining radiosensitivity *in vitro* is the clonogenic survival assay, which measures the consequences of radiation on the proliferative potential of individual cells. The radioresponse of human brain tumor xenografts, however, is typically defined according to animal survival and more recently using imaging techniques to define tumor growth rate, both of which are highly dependent on the number of tumor cells (clonogens) at the time of irradiation and in essence evaluate the radiosensitivity of the tumor cell population as a whole. Thus, to quantitatively compare the intrinsic radioresponse of tumor cells within ic xenografts to that of cells maintained under *in vitro* growth conditions we used γH2AX foci, which provides a sensitive measure of radiation-induced DNA DSBs (15). The dispersal of γH2AX foci reflects DSB repair with the residual foci remaining at 24h after irradiation having been shown to correlate with radiation-induced cell death, i.e. radiosensitivity. Whereas the relationship between residual γH2AX expression and radiosensitivity has been best established using in vitro models (5,16,17,29), the correlation has also been reported after *in vivo* irradiation of human tumor xenografts (17) as well as mouse normal tissue(18,30). The data reported here indicate that for two GBM TSC lines the dispersal of radiation-induced γH2AX foci was faster in cells within ic xenografts as compared to cells grown *in vitro*. These results then suggest that the GBM cells have a greater capacity to repair DSB when grown under orthotopic conditions, indicative of radioresistance as compared to their in vitro counterparts. In contrast to the ROS/ARE genes, there was not a consistent increase in the expression of DNA repair related genes in the *in vivo* versus *in vitro* models (data not shown). Thus, at present, the mechanism responsible for the enhanced repair capacity in GBM cells under orthotopic conditions remains to be defined.

GBM cells irradiated under ic conditions were also substantially less susceptible to γH2AX induction than cells grown *in vitro*. Differences in cell cycle phase distribution are unlikely to account for this effect: similar results were obtained when comparing cells grown orthotopically to cells *in vitro* that were cycling (those grown in stem cell media) and those arrested in G0/G1 (those grown in differentiation media). Alternatively, γH2AX induction *in vitro* can be overestimated when cells are irradiated on glass slides due the photo-electric effect and the generation of secondary radiation particles (31), which was suggested as a potential explanation for the fewer γH2AX foci induced in mouse normal tissue as compared to mouse cells *in vitro* (18). However, in our studies radiation was delivered *in vitro* and *in vivo* using a 320 kV X-irradiator, eliminating the contribution of the photo-electric effect and the possible overestimation of γH2AX induction *in vitro*. Finally, whereas a reduction in the maximum number of γH2AX foci induced could also be the result of relative decreases in H2AX expression and/or the expression of H2AX kinases (e.g. ATM, DNA-PK) (5), similar reductions were detected in the initial number 53BP1 foci induced ic, which provides an independent measure of DSB induction (28).

Thus, at this point data suggest that the reduced γH2AX and 53BP1 foci induction in ic xenografts may be the result of fewer DNA DSBs. It has been reported that radiation-inducedγH2AX expression was 3–4 times greater in well-oxygenated cells as compared to anoxic cells, with 0.55% oxygen producing a half-maximal response (32). With respect to the study presented here, anoxia as well as 0.55% oxygen would be expected to result in necrosis. Although areas of necrosis are present in the ic xenografts, γH2AX and 53BP1 foci

were evaluated only in healthy appearing tumor tissue (non-necrotic) with a relatively uniform response across tumors. Thus, it appears unlikely that the reduced level of foci induction detected after ic irradiation can be solely attributed to radiobiological hypoxia (~0.5%) (33). An additional determinant of DNA DSB induction and consequently radiosensitivity is cellular/tissue anti-oxidant capacity (34). Accordingly, enzymatic and non-enzymatic scavenging of ROS is well established to protect cells from radiation-induced DNA damage. Genes involved in ROS metabolism and anti-oxidant response were expressed at higher levels in ic xenografts than in the TSCs or their differentiated progeny *in vitro*. If this gene expression pattern translates to increased anti-oxidant capacity as described for breast tumor cells *in vitro* (35), the consequence would be reduced levels of DSBs after irradiation of orthotopic xenografts, consistent with reduced levels of radiation induced γH2AX and 53BP1. Of note, Pollard et al also recently showed that ROS scavengers reduced the levels of radiation-induced γH2AX foci in vitro, which was accompanied by a reduction in cytotoxicity (36).

The data presented here suggest that the brain microenvironment protects GBM cells from radiation-induced DSBs and facilitates their repair, a situation indicative of a relative decrease in intrinsic radiosensitivity. These results then imply that the microenvironment plays a major a role in mediating the radioresistance of GBMs. Although the relative decrease in susceptibility of ic xenografts to DSB induction can be linked to modifications in gene expression, the specific mechanisms through which the microenvironment regulates radiation-induced DNA damage and repair, and thus radiosensitivity, remain the subject of future investigations. However, based on these results it appears that for preclinical studies aimed at the identification of targets for GBM radiosensitization and the evaluation of corresponding radiosensitizers it will be necessary to account for the brain microenvironment.

Translational Relevance

Glioblastomas (GBMs) are one of the most radioresistant of human tumors. However, GBM cell lines grown *in vitro*, including GBM tumor stem like cells, do not display comparable radioresistance. In an attempt to account for this discrepancy, we compared the radioresponse of GBM tumor stem-like cells grown *in vitro* and as orthotopic xenografts using γH2AX and 53BP1 nuclear foci. The data presented suggest that tumor cells within the orthotopic xenografts have an increased capacity to repair DNA double strand breaks and are less susceptible to their induction as compared to cells grown *in vitro*. These results implicate the brain microenvironment as a source of GBM radioresistance. Moreover, this work suggests that preclinical studies aimed at developing radiosensitizers for GBM treatment need to take into account the brain microenvironment.

Supplementary Material

Refer to Web version on PubMed Central for supplementary material.

Acknowledgments

This work was supported by grant CA138519 from the National Institute of Health (PJT) and a Cancer Center Support Grant issued to Moffitt Cancer Center from the National Cancer Institute

References

1. Stupp R, Mason WP, van den Bent MJ, et al. Radiotherapy plus concomitant and adjuvant temozolomide for glioblastoma. N Engl J Med. 2005; 352:987–96. [PubMed: 15758009]

2. Chan JL, Lee SW, Fraass BA, et al. Survival and failure patterns of high-grade gliomas after three-dimensional conformal radiotherapy. J Clin Oncol. 2002; 20:1635–42. [PubMed: 11896114]
3. Hochberg FH, Pruitt A. Assumptions in the radiotherapy of glioblastoma. Neurology. 1980; 30:907–11. [PubMed: 6252514]
4. Li A, Walling J, Kotliarov Y, et al. Genomic changes and gene expression profiles reveal that established glioma cell lines are poorly representative of primary human gliomas. Mol Cancer Res. 2008; 6:21–30. [PubMed: 18184972]
5. MacPhail SH, Banath JP, Yu TY, Chu EH, Lambur H, Olive PL. Expression of phosphorylated histone H2AX in cultured cell lines following exposure to X-rays. Int J Radiat Biol. 2003; 79:351–8. [PubMed: 12943243]
6. Singh SK, Hawkins C, Clarke ID, et al. Identification of human brain tumour initiating cells. Nature. 2004; 432:396–401. [PubMed: 15549107]
7. Son MJ, Woolard K, Nam DH, Lee J, Fine HA. SSEA-1 is an enrichment marker for tumor-initiating cells in human glioblastoma. Cell Stem Cell. 2009; 4:440–52. [PubMed: 19427293]
8. Salmaggi A, Boiardi A, Gelati M, et al. Glioblastoma-derived tumorospheres identify a population of tumor stem-like cells with angiogenic potential and enhanced multidrug resistance phenotype. Glia. 2006; 54:850–60. [PubMed: 16981197]
9. Vescovi AL, Galli R, Reynolds BA. Brain tumour stem cells. Nat Rev Cancer. 2006; 6:425–36. [PubMed: 16723989]
10. McCord AM, Jamal M, Williams ES, Camphausen K, Tofilon PJ. CD133+ glioblastoma stem-like cells are radiosensitive with a defective DNA damage response compared with established cell lines. Clin Cancer Res. 2009; 15:5145–53. [PubMed: 19671863]
11. Galli R, Binda E, Orfanelli U, et al. Isolation and characterization of tumorigenic, stem-like neural precursors from human glioblastoma. Cancer Res. 2004; 64:7011–21. [PubMed: 15466194]
12. Lee J, Kotliarova S, Kotliarov Y, et al. Tumor stem cells derived from glioblastomas cultured in bFGF and EGF more closely mirror the phenotype and genotype of primary tumors than do serum-cultured cell lines. Cancer Cell. 2006; 9:391–403. [PubMed: 16697959]
13. Yuan X, Curtin J, Xiong Y, et al. Isolation of cancer stem cells from adult glioblastoma multiforme. Oncogene. 2004; 23:9392–400. [PubMed: 15558011]
14. Bonner WM, Redon CE, Dickey JS, et al. GammaH2AX and cancer. Nat Rev Cancer. 2008; 8:957–67. [PubMed: 19005492]
15. Lobrich M, Shibata A, Beucher A, et al. gammaH2AX foci analysis for monitoring DNA double-strand break repair: strengths, limitations and optimization. Cell Cycle. 9:662–9. [PubMed: 20139725]
16. Banath JP, Macphail SH, Olive PL. Radiation sensitivity, H2AX phosphorylation, and kinetics of repair of DNA strand breaks in irradiated cervical cancer cell lines. Cancer Res. 2004; 64:7144–9. [PubMed: 15466212]
17. Klokov D, MacPhail SM, Banath JP, Byrne JP, Olive PL. Phosphorylated histone H2AX in relation to cell survival in tumor cells and xenografts exposed to single and fractionated doses of X-rays. Radiother Oncol. 2006; 80:223–9. [PubMed: 16905207]
18. Rube CE, Grudzenski S, Kuhne M, et al. DNA double-strand break repair of blood lymphocytes and normal tissues analysed in a preclinical mouse model: implications for radiosensitivity testing. Clin Cancer Res. 2008; 14:6546–55. [PubMed: 18927295]
19. Jiang H, Gomez-Manzano C, Aoki H, et al. Examination of the therapeutic potential of Delta-24-RGD in brain tumor stem cells: role of autophagic cell death. J Natl Cancer Inst (2007/09/13). 2007:1410–4. [PubMed: 17848677]
20. Louis DN, Ohgaki H, Wiestler OD, et al. The 2007 WHO classification of tumours of the central nervous system. Acta Neuropathol. 2007; 114:97–109. [PubMed: 17618441]
21. McCord AM, Jamal M, Shankavaram UT, Lang FF, Camphausen K, Tofilon PJ. Physiologic oxygen concentration enhances the stem-like properties of CD133+ human glioblastoma cells in vitro. Mol Cancer Res. 2009; 7:489–97. [PubMed: 19372578]
22. Van Gelder RN, von Zastrow ME, Yool A, Dement WC, Barchas JD, Eberwine JH. Amplified RNA synthesized from limited quantities of heterogeneous cDNA. Proc Natl Acad Sci U S A. 1990; 87:1663–7. [PubMed: 1689846]

23. Irizarry RA, Hobbs B, Collin F, et al. Exploration, normalization, and summaries of high density oligonucleotide array probe level data. Biostatistics. 2003; 4:249–64. [PubMed: 12925520]
24. Kohonen, T. Self-Organizing Maps. Berlin: Springer; 1995.
25. Tothova Z, Gilliland DG. FoxO transcription factors and stem cell homeostasis: insights from the hematopoietic system. Cell Stem Cell. 2007; 1:140–52. [PubMed: 18371346]
26. Wang X, Tomso DJ, Chorley BN, et al. Identification of polymorphic antioxidant response elements in the human genome. Hum Mol Genet. 2007; 16:1188–200. [PubMed: 17409198]
27. Schultz LB, Chehab NH, Malikzay A, Halazonetis TD. p53 binding protein 1 (53BP1) is an early participant in the cellular response to DNA double-strand breaks. J Cell Biol. 2000; 151:1381–90. [PubMed: 11134068]
28. Celeste A, Fernandez-Capetillo O, Kruhlak MJ, et al. Histone H2AX phosphorylation is dispensable for the initial recognition of DNA breaks. Nat Cell Biol. 2003; 5:675–9. [PubMed: 12792649]
29. Olive PL. Detection of DNA damage in individual cells by analysis of histone H2AX phosphorylation. Methods Cell Biol. 2004; 75:355–73. [PubMed: 15603433]
30. Bhogal N, Kaspler P, Jalali F, et al. Late residual gamma-H2AX foci in murine skin are dose responsive and predict radiosensitivity in vivo. Radiat Res. 173:1–9. [PubMed: 20041754]
31. Kegel P, Riballo E, Kuhne M, Jeggo PA, Lobrich M. X-irradiation of cells on glass slides has a dose doubling impact. DNA Repair (Amst). 2007; 6:1692–7. [PubMed: 17644493]
32. Olive PL, Banath JP. Phosphorylation of histone H2AX as a measure of radiosensitivity. Int J Radiat Oncol Biol Phys. 2004; 58:331–5. [PubMed: 14751500]
33. Sattler UG, Mueller-Klieser W. The anti-oxidant capacity of tumour glycolysis. Int J Radiat Biol. 2009; 85:963–71. [PubMed: 19895273]
34. Sonntag, VC. The chemical basis of radiation biology. Taylor and Francis Press; N.Y: 1987.
35. Diehn M, Cho RW, Lobo NA, et al. Association of reactive oxygen species levels and radioresistance in cancer stem cells. Nature. 2009; 458:780–3. [PubMed: 19194462]
36. Pollard JM, Reboucas JS, Durazo A, et al. Radioprotective effects of manganese-containing superoxide dismutase mimics on ataxia-telangiectasia cells. Free radical biology & medicine. 2009; 47:250–60. [PubMed: 19389472]

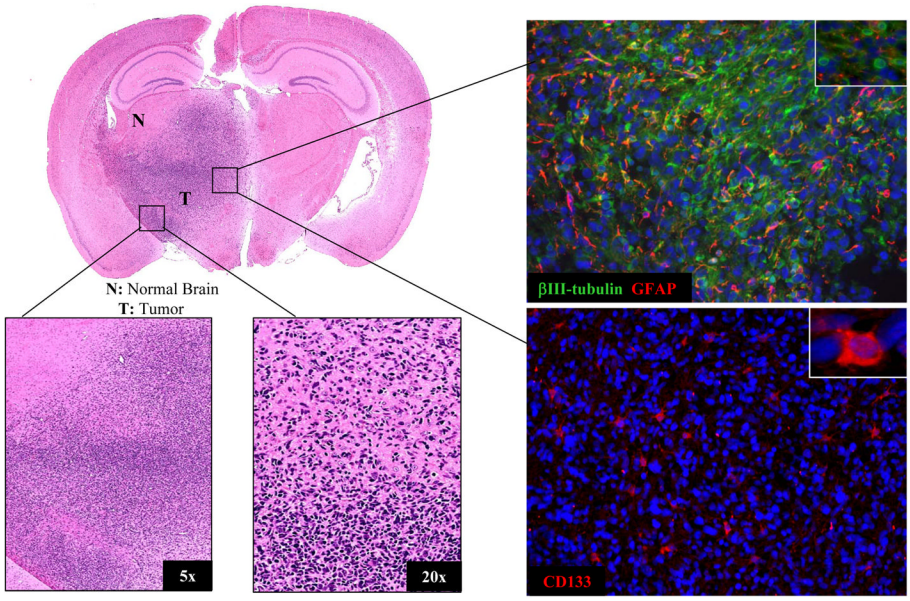

Figure 1. Intracerebral (ic) xenograft initiated from CD133+ NSC11 TSCs

A representative mouse was euthanized at the initial signs of morbidity (49 days after implantation); the brain tumor was then prepared for histological analyses. Left panels: H&E staining; Right panels: immunoflorescent analyses of GFAP, βIII tubulin and CD133 expression with nuclei counterstained with DAPI (blue); 20x magnification with insert at 63x.

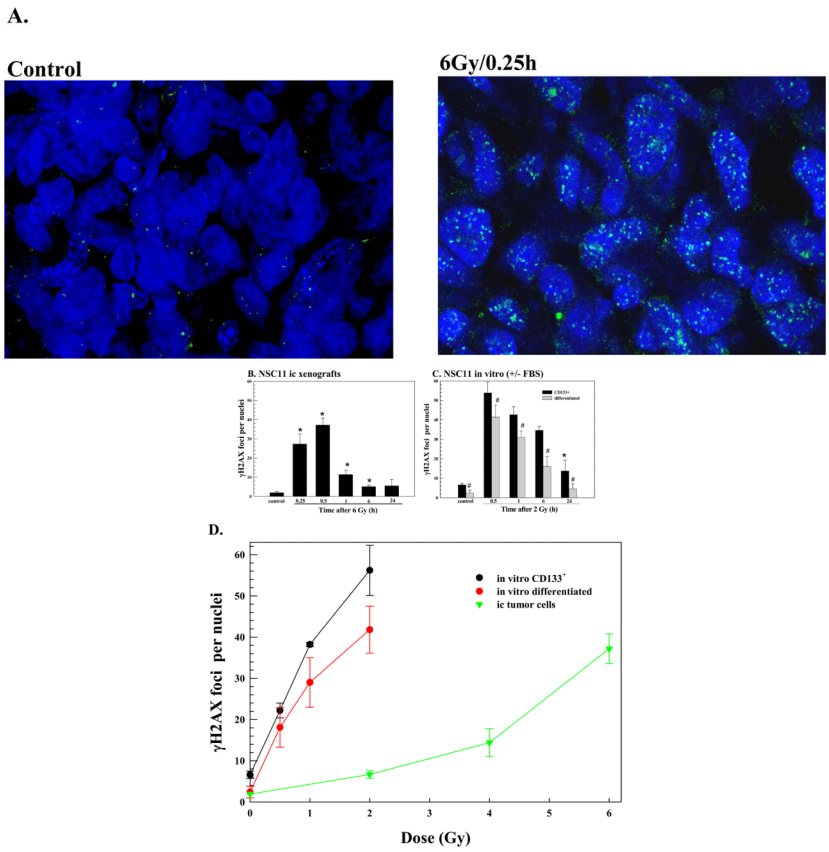

Figure 2. γH2AX foci after irradiation of NSC11 cells: *in vivo* (ic) versus *in vitro*

(A) Intracerebral xenografts initiated from CD133+ NSC11 cells were locally irradiated (6Gy) at the initial signs of morbidity (42–49 days after implantation). Representative maximum projection confocal micrographs (63x magnification) of γH2AX nuclear foci (green) in ic tumor xenografts at 0.25h after 6 Gy. (B) γH2AX foci induction and dispersal after irradiation of ic xenografts. Values shown represent the mean ± SD of 3–4 mice in which 50 tumor cells were scored per mouse. * $p < 0.05$ as compared to unirradiated control. (C) Monolayer cultures of CD133+ NSC11 cells grown in stem-cell media (black bars) or 10% FBS (gray bars) were irradiated (2 Gy) and analyzed at the specified times. Values shown represent the mean ± SD of 3 independent experiments in which 50 cells were scored per time point. * $p < 0.05$ as compared to unirradiated control; # $p<0.05$ as compared to CD133+ cells. (D) γH2AX foci induced at 0.5h as a function of radiation dose for the three growth conditions. For the *in vitro* conditions values represent the mean ± SD of 3 independent experiments in which 50 cells were evaluated per dose; the 2 Gy value is the same as shown in the time course analysis (C). For the ic xenografts values represent the mean ± SD for 3–4 mice in which 50 tumor cells were scored per mouse; the 6 Gy value is the same as shown in (B).

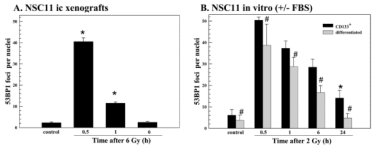

Figure 3. 53BP1 foci after irradiation of NSC11 cells: *in vivo* (ic) vs. *in vitro*

Intracerebral xenografts initiated from CD133+ NSC11 cells were locally irradiated (6Gy) at the initial signs of morbidity (42–49 days after implantation). (A) 53BP1 foci induction and dispersal after irradiation of ic xenografts. Values shown represent the mean ± SD of 3–4 mice in which 50 tumor cells were scored per mouse. * $p < 0.05$ as compared to unirradiated control. (B) monolayer cultures of CD133+ NSC11 cells grown in stem-cell media (black bars) or 10% FBS (gray bars) were irradiated (2 Gy) and analyzed at the specified times. Values shown represent the mean ± SD of 3 independent experiments in which 50 cells were scored per time point. * $p < 0.05$ as compared to unirradiated control; # $p<0.05$ as compared to CD133+ cells.

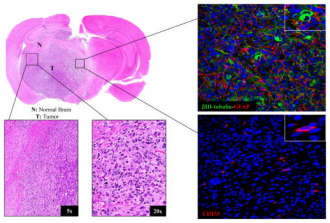

Figure 4. Intracerebral (ic) xenograft initiated from CD133+ GBMJ1 TSCs

A representative mouse was euthanized at the initial signs of morbidity (94 days after implantation); the brain tumor was then prepared for histological analyses. Left panels: H&E staining and Right panels: immunoflorescent analyses of GFAP, β-III tubulin and CD133 expression with nuclei counterstained with DAPI (blue); 20x magnification with insert at 63x.

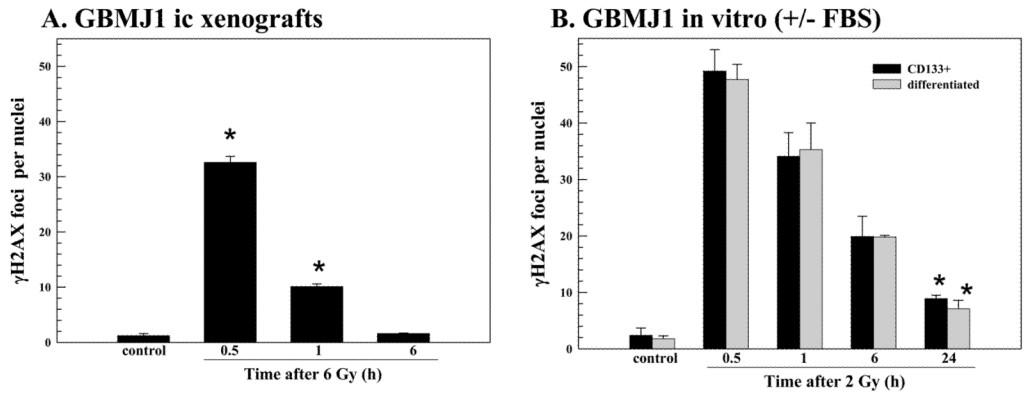

Figure 5. γH2AX foci after irradiation of GBMJ1 cells: *in vivo* (ic) vs. *in vitro*

Intracerebral xenografts initiated from CD133+ GBMJ1 cells were locally irradiated (6Gy) at the initial signs of morbidity (72–94 days after implantation). (A) γH2AX foci induction and dispersal after irradiation of ic xenografts. Values shown represent the mean ± SD of 3–4 mice in which 50 tumor cells were scored per mouse. (B) monolayer cultures of CD133+ GBMJ1 cells grown in stem-cell media (black bars) or 10% FBS (gray bars) were irradiated (2 Gy) and analyzed at the specified times. Values shown represent the mean ± SD of 3 independent experiments in which 50 cells were scored per time point. * $p < 0.05$ as compared to unirradiated control

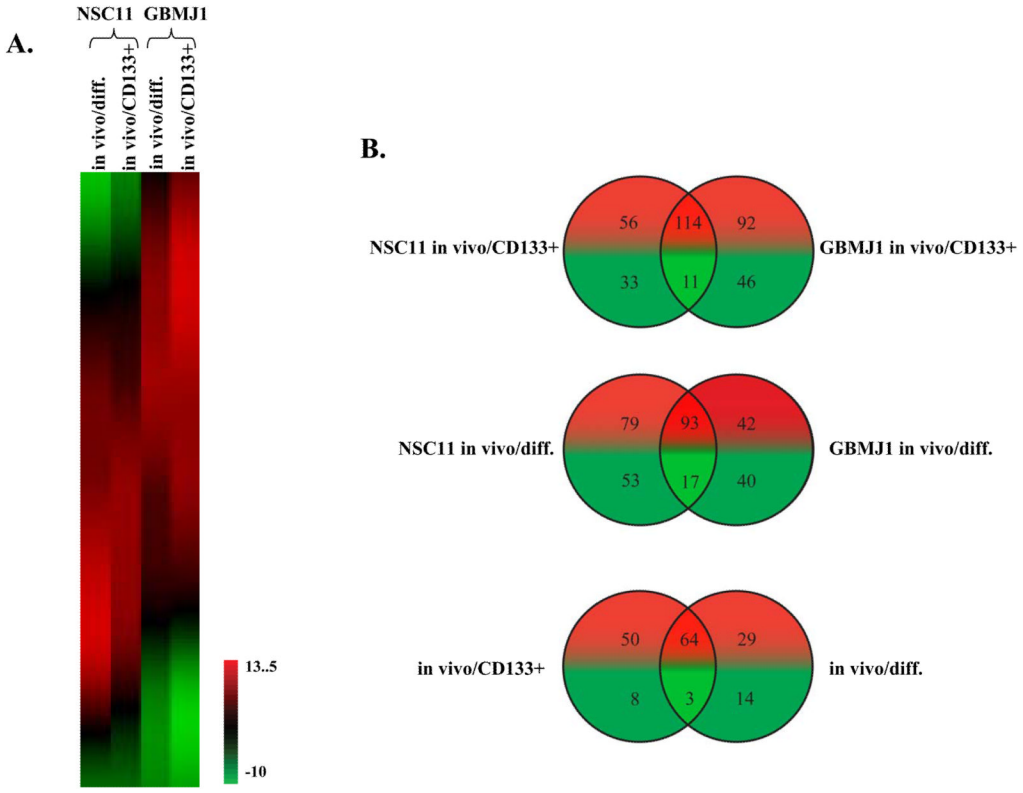

Figure 6. Influence of ic growth on gene expression

Microarray analysis was preformed on NSC11 and GBMJ1 TSCs grown under 2 *in vitro* conditions (CD133+ and differentiated) and as ic xenografts. The effect of ic growth was determined by directly comparing expression levels between each ic xenografts and their respective *in vitro* cultures. (A) SOM generated using all Affymetrix-probsets and the log2-transformed fold-change expression levels comparing ic xenografts to *in vitro* growth conditions (CD133+ and differentiated). The expression indicator refers to log2 changes. (B) Venn diagram for ROS/ARE related genes. Genes whose expression was modified by at least 2-fold (increase or decrease) were filtered through a ROS/ARE-related gene list (Supplemental Table 1) and compared using Venn diagrams. The top and middle panels show Venn diagrams of increased (red) and decreased (green) ROS/ARE genes from the two ic xenografts as compared to their *in vitro* CD133+ and differentiated cultures, respectively. The bottom panel shows a Venn diagram comparing the genes affected by ic growth for each *in vitro* culture condition. The commonly affected genes in CD133+ and differentiated cultures in both GBM models are shown in Supplemental Table 2.